Journal of Bionic Engineering (2022) 19:1024–1035
https://doi.org/10.1007/s42235-022-00176-2

RESEARCH ARTICLE

Study on Functional Mechanical Performance of Honeycomb Array Structures Inspired by Gideon Beetle

Ruiyao Liu[1] · Guofeng Yao[1] · Zezhou Xu[2] · Xue Guo[2] · Kuiyang Gao[1] · Qing Cao[2] · Zhenglei Yu[2,3] · Zhihui Zhang[2] · Chunyang Han[4] · Jiabao Liu[5]

Received: 8 November 2021 / Revised: 21 January 2022 / Accepted: 29 January 2022 / Published online: 28 March 2022

Abstract

To obtain bio-inspired structures with superior biological function, four bio-inspired structures named regular arrangement honeycomb structure (RAHS), staggered arrangement honeycomb structure (SAHS), floral arrangement honeycomb structure (FLAHS) and functional arrangement honeycomb structure (FUAHS) are designed by observing the microstructure of the Gideon beetle, based on the optimal size bio-inspired cells by response surface method (RSM) and particle swarm optimization (PSO) algorithm. According to Euler theory and buckling failure theory, compression deformation properties of bio-inspired structures are explained. Experiments and simulations further verify the accuracy of theoretical analysis results. The results show that energy absorption of FLAHS is, respectively, increased by 26.95%, 22.85%, and 121.45%, compared with RAHS, SAHS, and FUAHS. Elastic modulus of FLAHS is 110.37%, 110.37%, and 230.56% of RAHS, SAHS, and FUAHS, respectively. FLAHS perfectly inherits crashworthiness and energy absorption properties of the Gideon beetle, and FLAHS has the most stable force. Similarly, RAHS, SAHS, and FUAHS, respectively, inherit mechanical properties of the Gideon beetle top horn, the Gideon beetle middle horn, and the abdomen of the beetle. This method, designing bio-inspired structures with biological functions, can be introduced into the engineering field requiring the special function.

Keywords Bionic structural design · Optimal size design · Euler theory · Buckling and failure theory · Additive manufacturing

1 Introduction

With the development of anti-impact structures, researchers have designed all kinds of novel optimization structures for various engineering fields, such as automobile anti-collision beams, packaging boxes, honeycomb panels of shipping skins, and so on [1–4]. In all of these designs, lightweight and protection properties are crucial. In addition, the optimization and functional characteristics of structural parts in various directions have become mainstream [5–7]. Demanding functional structures are designed and manufactured by imitating the natural biological structures, such as honeycomb structures, bamboo structures, and so on [8–12].

In the past decades, researchers have made significant achievements in structural bending [13], structural energy absorption [14], structural bearing capacity [15], structural dynamic response [16], and high and low-temperature structural performance [17]. In a variety of structural performance comparison, honeycomb structures have superior properties. Gibson et al. [18] established a theoretical model for

✉ Zhenglei Yu
zlyu@jlu.edu.cn

1 Department of Mechanics, School of Mechanical and Aerospace Engineering, Jilin University, Changchun 130022, China

2 Key Laboratory of Engineering Bionics, Ministry of Education, Jilin University, Changchun 130022, China

3 Key Laboratory for Cross-Scale Micro and Nano Manufacturing, Ministry of Education, Changchun University of Science and Technology, Changchun 130000, China

4 Changchun Institute of Optics, Fine Mechanics and Physics, Chinese Academy of Sciences, Changchun 130022, China

5 Archives, Jilin Construction University, Changchun 130000, China

calculating honeycomb for linear elastic, non-linear elastic, and plastic behavior. Zhang et al. [19] studied the deformation mechanism and energy absorption performance of different honeycomb structures under low-speed impact through experiments and numerical simulation. For the morphological defect, Chen et al. [20] systematically considered its effect on the yield performance of two-dimensional honeycomb under biaxial loading and presented a new method of replacing defects with holes. To study the influence of different defects on structures, Asprone et al. [21] studied the performance of honeycomb structures, and the predicted structural response had a good correlation with the experimental results by numerical calculation with different defects sets. Wang et al. [22] conducted an in-depth study on the crushing behavior of random honeycomb cylindrical shells. Similarly, with the research of complex three-dimensional honeycomb structures, the manufacturing methods of complex structures are likewise gradually changing. The development of 3D-printing technology simplifies the manufacturing process to a considerable extent [23–25]. 3D-printing technology is used for structural manufacturing in various scientific types of researches [26]. In this paper, four bio-inspired structures are manufactured with 3D-printing technology.

In this study, three-dimensional honeycomb cells with excellent performance are designed and the effects of structural parameters on mechanical properties are analyzed. The optimal size of the honeycomb cell is obtained through RSM and PSO algorithm. According to the orderly arrangement of the Gideon beetle top horn, the staggered arrangement of the Gideon beetle middle horn, the overlapping arrangement of the Gideon beetle shard, and the symmetrical arrangement of the Gideon beetle abdominal layers, four honeycomb arrangement structures are designed: regular arrangement honeycomb structure (RAHS), staggered arrangement honeycomb structure (SAHS), floral arrangement honeycomb structure (FLAHS) and functional arrangement honeycomb structure (FUAHS). The mechanical properties of bio-inspired honeycomb arrangement structures are studied by experiments, simulations, and theories. All results are utilized to ensure the functional properties of honeycomb arrangement structures.

2 The Optimal Size Design of Bio-Inspired Honeycomb Arrangement Structures

2.1 Material Properties

In this study, the 3D-printing FS 3300PA machine is used to manufacture complex bio-inspired structures. The structural material is nylon. Different 3D-printing parameters seriously influence the structural forming quality and nylon structural mechanical properties. To meet the requirements of impact resistance of structures, Nylon tensile samples and bio-inspired structures are manufactured using the same 3D printing parameters. 3D-printing parameters are volume forming rate (L/h), scanning speed (m/s), build cavity temperature (°F), and laser power (W), and powder layer thickness (mm). 3D printing parameters are shown in Table 1, and the tensile experiments are carried out on the tensile samples. The stress–strain curves of nylon tensile samples are obtained, as shown in Fig. 1.

Table 1 FS 3300PA 3D-printing parameters

Parameters	Volume forming rate (L/h)	Scanning speed (m/s)	Build cavity temperature (°F)	Laser power (W)	Powder layer thickness (mm)
Tensile sample	75	7.6	6422	30	0.12

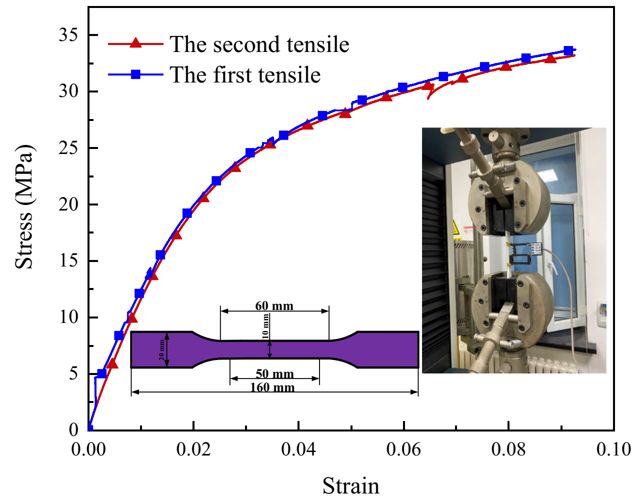

Fig. 1 The stress–strain curves of 3D-printed tensile samples. 50 mm is the original gauge length of tensile samples, and 60 mm is the parallel length of tensile samples. The tensile samples' thickness is 4 mm

In all of our calculations, the elastic modulus of materials is E, $E = 1000$ Mpa, poisson's ratio $\upsilon = 0.39$, and density $D = 0.95\ \mathrm{g/cm^3}$, which are typical properties of Nylon. To ensure the accuracy of simulation calculations, #24 elastoplastic material is selected for simulation calculation because the material tensile curve can be directly imported into #24 material for simulation calculation.

2.2 Design and Selection of Honeycomb Cell

The honeycomb cell has excellent impact resistance and energy absorption properties. The three-dimensional honeycomb cell is shown in Fig. 2a. The honeycomb cell has different energy absorption and protection properties at different sizes. Given this phenomenon, the optimal

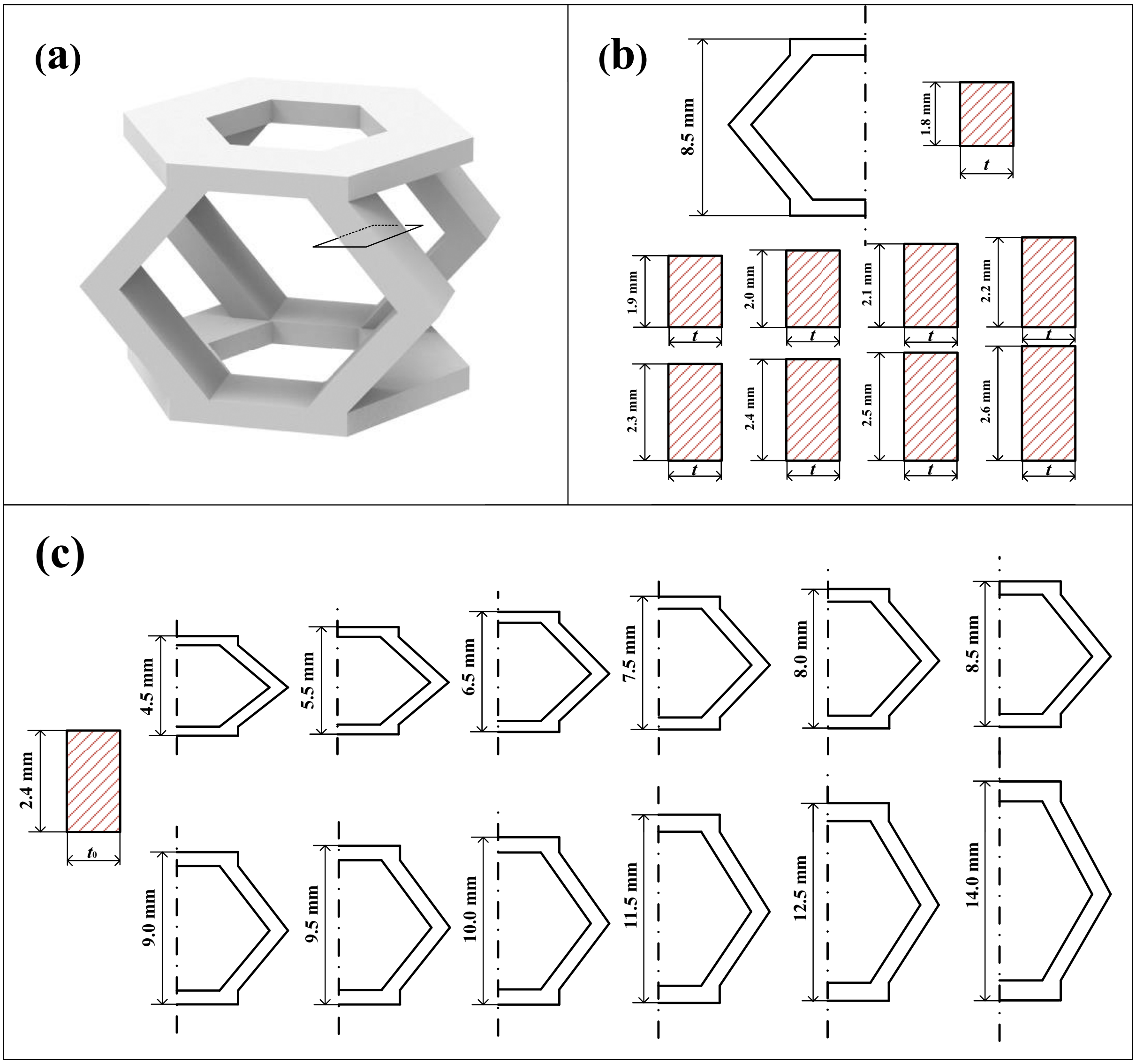

Fig. 2 The novel three-dimensional honeycomb cell structure. **a** The 3D model of honeycomb cell. **b** The 2D cross-section cut from (**a**). Due to the limitation of 3D-printing equipment, the structure section thickness is $t = 0.8$ mm and the section width size is changed. **c** When the section size is fixed, the height of the honeycomb cell changes discretely and the section thickness is $t_0 = 1$ mm

three-dimensional honeycomb cell is obtained by changing structural cell wall thickness and cell height with discrete variables, as shown in Fig. 2b, c.

The honeycomb cells with different heights and width are compressed, and the cell compression amount is all 30% of their height. The crush peak force (CPF), crush mean force (CMF), energy absorption (EA), and specific energy absorption (SEA) of different parameters cell structures are obtained by compression simulation of the honeycomb cells, as shown in Fig. 3a_1–d_1 and a_2–d_2.

The results show that the CPF of bio-inspired cells decreases with the increase of the cell height. EA and SEA of bio-inspired cells show a Mongolian bag, and *EA* is optimal when the height of the bio-inspired cell is 7–9 mm, as shown in Fig. 3a_1–d_1. CPF and CMF of cells with different discrete widths gradually increase and show a linear state. EA and *SEA* are constant and only show a slight linear increase state, as shown in Fig. 3a_2–d_2.

To find the optimal cell size, particle swarm optimization (PSO) and response surface (RSM) are used [27–29].

$$\begin{cases} \max\ :\ f(x) = f(x_1, x_2, x_3) \\ \quad s.t. x_1 \in (0, 20) \\ \quad\quad x_2 \in (0, 4) \\ \quad\quad\quad x_3 > 0 \end{cases}, \quad (1)$$

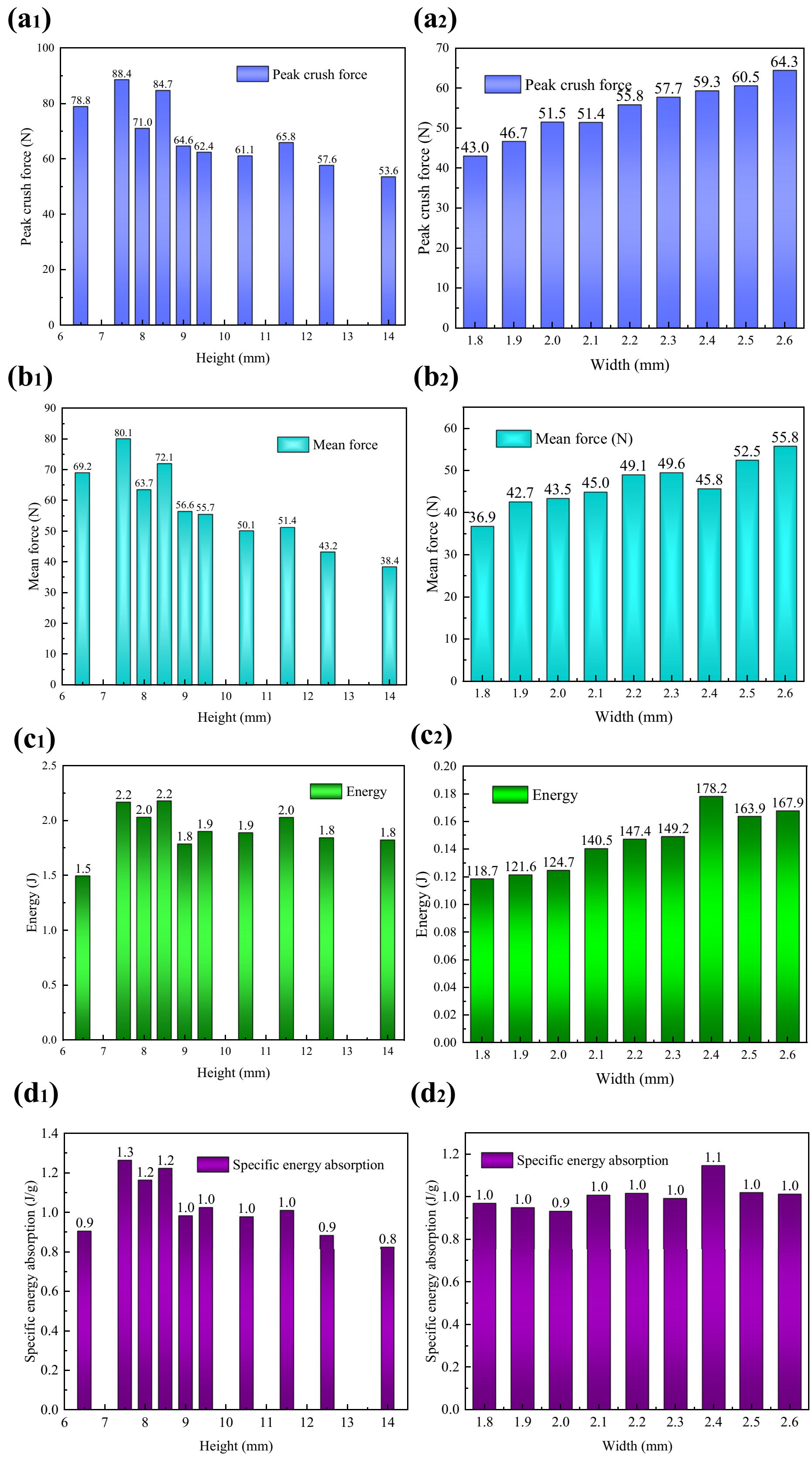

Fig. 3 Compression properties comparison of different parameters cell structures. $\mathbf{a_1}$–$\mathbf{d_1}$ show mechanical properties when the cell's height changes, and $\mathbf{a_2}$–$\mathbf{d_2}$ show mechanical properties when the cell's truss width changes

where, x_1 is the height of the cell structure. x_2 is the width of the cell structure, and x_3 is the thickness of the structural cell rod. $f(x)$ is SEA because SEA is the most representative parameter.

The prediction function is

$$f(x) = ux_2 + w\sin x_1 + c\sin x_2 + dx_1^2 + ex_2^2 + fx_3^2 + gx_1^3 + hx_2^3 + rx_3^3 + s. \tag{2}$$

In the particle swarm optimization algorithm, the initial population number is set as 320 and the number of adjacent populations is set as 15. The learning factor is set as 2.1, and the prediction function is obtained

$$\begin{aligned} f(x) = {} & -0.68338x_2 + 0.05176\sin x_1 + 2.86105\sin x_2 + 0.01382x_1^2 - 1.49202x_2^2 \\ & + 1.11241x_3^2 - 0.0001x_1^3 + 0.61372x_2^3 - 0.44637x_3^3 - 0.1163. \end{aligned} \tag{3}$$

It can be seen from Fig. 4b that the honeycomb cell structure with a height of 8.5 mm and a width of 2.4 mm has the best energy absorption properties. Therefore, the honeycomb cell, with a height of 8.5 mm and a beam cross-section width of 2.4 mm, is selected for the bio-inspired layout design.

2.3 Design of Bio-Inspired Honeycomb Arrangement Structures Based on Gideon Beetle

In nature, the Gideon beetle can lift or move heavy objects dozens or hundreds of times heavier than itself with its horns, which means its horns have excellent hardness, strength, and bending resistance [30, 31]. And Gideon beetle, which lives in trees several meters high, is at risk of falling or being hit by hard objects, but their evolved elytra and abdomen attached to a piece of bone protect them from such risks, which means its elytra and abdomen have excellent impact resistance and energy absorption properties. To get bio-inspired structures that have excellent functional characteristics of various parts of the Gideon beetle, the bio-inspired design is implemented by mimicking the microscopic pictures of the various parts of the Gideon beetle in this study. Fig. 5b–e are obtained by using the scanning electron microscope (XL-30 ESEM FEG). It can be seen that cell structures of the top horn in Fig. 5b are arranged neatly, and cell structures of the middle horn in Fig. 5c are staggered, and cell structures of the shard in Fig. 5d are staggered between layers, and cell structures of the abdomen in Fig. 5e are curved and symmetrical. According to the orderly arrangement of the top horn of the Gideon beetle, the staggered arrangement of the middle horn, the overlapping arrangement of the shard, and the symmetrical arrangement at the angle of rotation

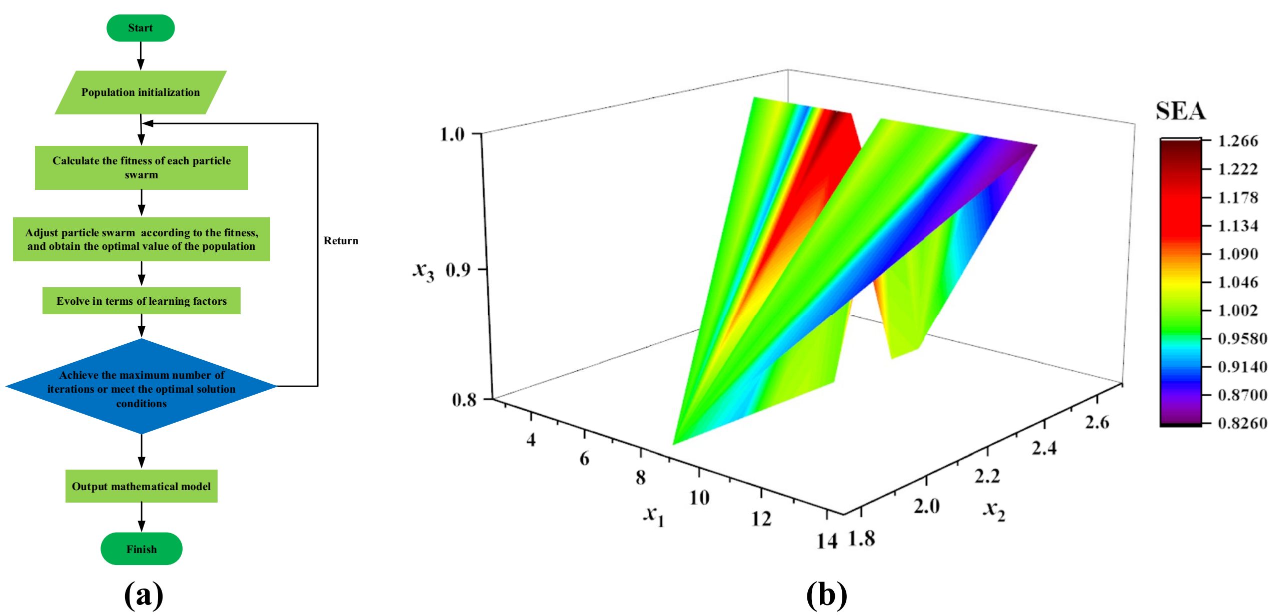

Fig. 4 **a** PSO flow chart. **b** Surface diagram of *SEA* optimization model. In **b**, x_1, x_2 and x_3 represent height, width and SEA, respectively

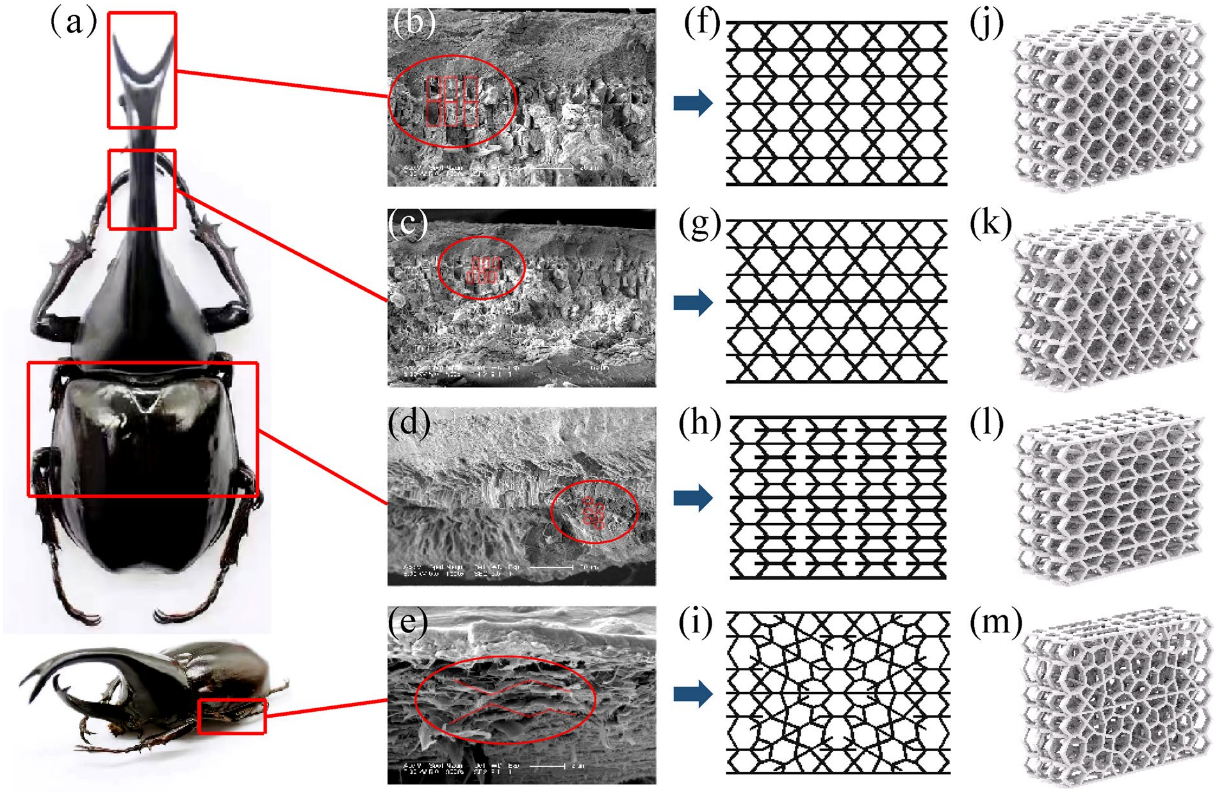

Fig. 5 Four bio-inspired honeycomb structures. **a** A profile view of the Gideon beetle. **b** Scanning electron microscopy of Gideon beetle horn tip. **c** Scanning electron microscope on the middle part of the beetle horn. **d** Scanning electron microscopy of the beetle shard. **e** Scanning electron microscopy of the beetle abdomen. **f** The regular arrangement honeycomb structure (RAHS) inspired by (**b**). **g** The staggered arrangement honeycomb structure (SAHS) is inspired by (**c**). **h** The floral arrangement honeycomb structure (FLAHS) is inspired by (**d**). (i) The functional arrangement honeycomb structure (FUAHS) is inspired by (e). **j**–**m** The three-dimensional solid structure corresponding to **f**–**i**

between the abdominal layers, four bio-inspired structures are designed based on the optimal honeycomb cell: RAHS, SAHS, FLAHS, and FUAHS, as shown in Fig. 5f–i.

3 Theoretical Analysis of Quasi-Static Compression

In the whole process of structural compression, assume that bio-inspired structures conform to the Euler beam theory before elastic buckling. First, the relative density of honeycomb structures is

$$\rho_r = \frac{V_{str}}{V_s}\rho_s, \tag{4}$$

where, ρ_r is the equivalent density of the three-dimensional honeycomb structure. ρ_s is material density of the three-dimensional honeycomb structure. V_{str} is the solid volume of the three-dimensional honeycomb structure. V_s is the overall volume of the three-dimensional honeycomb structure.

According to the geometric relationship, the structural volume is

$$V_{beam} = btl, \tag{5}$$

$$V_{ts} = \frac{bt_0\left(l_1 + l_2\right)}{2}, \tag{6}$$

$$V_{RAHS} = V_{SAHS} = V_{ts}\left[5ij(k+1) + (k+1)j\right] + 4V_{beam}kj(i+1), \tag{7}$$

$$V_{FLAHS} = V_{st}\left[5i\left[\frac{j+1}{2}\right](k+1) + (k+1)j\right] + t_0b\left(l_1 + l_3\right)(i+1)(k+1) + l_2bt_0k\left(\left[\frac{j+1}{2}\right] - 1\right)(i+1) \tag{8}$$

$$V_{\mathrm{FUAHS}} = \sum l_s t_m b \tag{9}$$

$$V_s = BTL, \tag{10}$$

where, V_{beam} is the volume of a single truss beam and b, t, l denotes width, thickness, and length, respectively. l_1, l_2 is the length of the outer and inner sides of the top hexahedron. l_3 is the length of a cell rod. t_0 is the thickness of the top hexahedron. i, j, and k is the number of deep, horizontal, and vertical directions. V_{ts} is the one-sixth top surface volume of the honeycomb cell.

Because of the complexity of FUAHS, the solid volume of FUAHS can be obtained directly by calculating the truss beam. Then the relative density is

$$\rho_{\mathrm{RAHS}} = \frac{V_{\mathrm{RAHS}}}{V_s}\rho_s, \tag{11}$$

$$\rho_{\mathrm{SAHS}} = \frac{V_{\mathrm{SAHS}}}{V_s}\rho_s, \tag{12}$$

$$\rho_{\mathrm{FLAHS}} = \frac{V_{\mathrm{FLAHS}}}{V_s}\rho_s, \tag{13}$$

$$\rho_{\mathrm{FUAHS}} = \frac{V_{\mathrm{FUAHS}}}{V_s}\rho_s = \frac{\sum l_s t_m b}{BTL}\rho_s. \tag{14}$$

Consider the compression force applied to honeycomb structures along the vertical positive direction. The honeycomb structures under stress can be simplified to beams as shown in Fig. 6. The torque M and compression force $F = \sigma A$ can be obtained from the equilibrium relationship.

$$F_{\mathrm{RAHS}} = F_{\mathrm{SAHS}} = \frac{\sigma V_{ts}(5ij + 5j)}{2t_0(j+1)(i+1)}, \tag{15}$$

$$F_{\mathrm{FLAHS}} = \frac{\sigma_{\mathrm{FLAHS}} b\left(L - l_1 \sin\theta\right)}{j+1} \tag{16}$$

$$F_{\mathrm{FUAHS}} = \sigma_{\mathrm{FUAHS}} A_{\mathrm{FUAHS}}, \tag{17}$$

$$M = \frac{Fl\sin\theta}{2}, \tag{18}$$

where, σ is stress operating on the cross section. A is the area of hexahedron on the top of the honeycomb cell. $I = \frac{bt^3}{12}$. E_s is the elastic modulus.

Strain of overall structures can be obtained as

$$\varepsilon_{\mathrm{RAHS},x} = \varepsilon_{\mathrm{SAHS},x} = \varepsilon_{\mathrm{FLAHS},x} = \frac{2ks\cos\theta}{H}, \tag{19}$$

$$\varepsilon_{\mathrm{FUAHS},x} = \frac{2k_e s_e \cos\theta}{H}, \tag{20}$$

$$\varepsilon_{\mathrm{RAHS},z} = \varepsilon_{\mathrm{SAHS},z} = \frac{2js\sin\theta}{L}, \tag{21}$$

$$\varepsilon_{\mathrm{FLAHS},z} = \frac{2(j+1)s\sin\theta}{L}, \tag{22}$$

$$\varepsilon_{\mathrm{FUAHS},z} = \frac{rs_e\sin\theta}{L}, \tag{23}$$

where, s_e, r and k_e are the deflection of FUAHS truss, the number of FUAHS horizontal top and vertical edge truss, respectively.

According to the definition formula of elastic modulus $E = \frac{\sigma}{\varepsilon_x}$ and poisson's ratio $\upsilon = -\frac{\varepsilon_x}{\varepsilon_z}$, the elastic modulus and poisson's ratio are

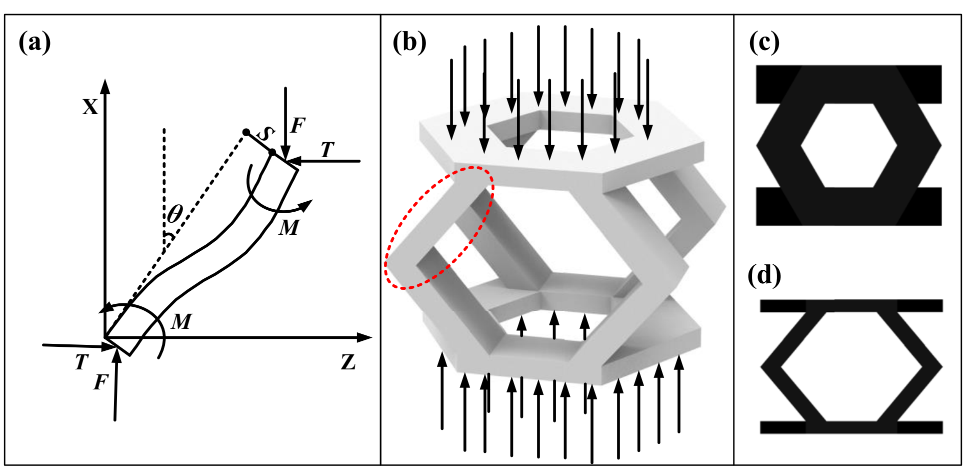

Fig. 6 The honeycomb structure buckling. **a** Euler beam buckling. **b** The honeycomb cell compression. **c** Top view of the honeycomb cell. **d** Front view of the honeycomb cell. $s = \frac{Fl^3\sin\theta}{12E_sI}$[34]

$$E_{\mathrm{RAHS}} = E_{\mathrm{SAHS}} = \frac{2(i+1)(j+1)\mathrm{H}E_s t^3}{(5ij+5j)kl^3\left(l_1+l_2\right)\sin\theta\cos\theta}, \tag{24}$$

$$E_{\mathrm{FLAHS}} = \frac{(j+1)\mathrm{H}E_s t^3}{2kl^3(L-l\sin\theta)}, \tag{25}$$

$$E_{\mathrm{FUAHS}} = \frac{\mathrm{H}E_s bt^3}{2k_e A_{\mathrm{FUAHS}} l^3 \sin\theta\cos\theta}, \tag{26}$$

$$\upsilon_{\mathrm{RAHS}} = \upsilon_{\mathrm{SAHS}} = -\frac{kL\cot\theta}{jH} \tag{27}$$

$$\upsilon_{\mathrm{FLAHS}} = -\frac{2kL\cot\theta}{(j+1)H} \tag{28}$$

$$\upsilon_{\mathrm{FUAHS}} = -\frac{2k_e L\cot\theta}{rH}. \tag{29}$$

As the compression continues, the structural force increases. The force on the truss reaches the critical force of structural instability, and the cell buckling occurs. The buckling force is

$$p_{\mathrm{cr}} = \frac{n^2\pi^2 E_s I}{l^2} = \frac{\pi^2 E_s I}{\eta^2 l^2}, \tag{30}$$

where assume that one end is fixed and the other end is hinged, $\eta = 0.7$.[16]

That is

$$F_{\mathrm{RAHS,cr}} = F_{\mathrm{SAHS,cr}} = ijp_{\mathrm{cr}}, \tag{31}$$

$$F_{\mathrm{FLAHS,cr}} = ijp_{\mathrm{cr},3}, \tag{32}$$

$$F_{\mathrm{FUAHS,cr}} = \sum_{N=1}^{M} p_{cr,N}. \tag{33}$$

After the occurrence of structural instability, the honeycomb structure gradually bends and deforms, and the force further increases, leading to structural failure. The force fluctuates around this failure force, and the failure force satisfies the identity.

$$4M_p\phi = 2p_{pl}\phi l\sin\theta, \tag{34}$$

$$M_p = \frac{1}{4}\sigma_{ys}bt^2, \tag{35}$$

$$p_{pl} = \frac{\sigma_{ys}bt^2}{2l\sin\theta}, \tag{36}$$

So

$$F_{\mathrm{RAHS,pl}} = F_{\mathrm{SAHS,pl}} = ijp_{\mathrm{pl}}, \tag{37}$$

$$F_{\mathrm{FLAHS,pl}} = ijp_{pl,3}, \tag{38}$$

$$F_{\mathrm{FUAHS,pl}} = \sum_{N=1}^{M} p_{pl,N}. \tag{39}$$

Through calculating, the information of four honeycomb arrangement structures is shown in Table 2.

By comparison with Fig. 8a, it can be seen that the theoretical analysis results have high accuracy and the error is guaranteed to be within 10%.

4 Bionic Structure Analysis

4.1 Performance Indicators

To accurately and quantitatively measure the energy absorption and protective performance of bio-inspired structures, some evaluation indicators are used in this paper, including energy absorption (EA), specific energy absorption (SEA), crush peak force (CPF), crush mean force (CMF), and crush force efficiency (CFE).

EA is the total energy absorbed during compression, shown in Eq. (40).

$$\mathrm{EA} = \int_0^{x_0} F dx, \tag{40}$$

where x_0 is the total quasi-static compression distance, F is quasi-static compression force and x is the instantaneous compression displacement.

Considering that mass is a critical indicator in bio-inspired structural design, SEA is as a high indicator of the energy absorbed per unit mass, as shown in Eq. (41). EA and SEA are extremely vital within applications of protective engineering.

$$\mathrm{SEA} = \frac{\mathrm{EA}}{M}, \tag{41}$$

where, M is the structural mass.

Table 2 The information of four honeycomb arrangement structures

Structure	Relative density	Elasticity modulus	Cell buckling force
RAHS	0.157	9.885	957.42
SAHS	0.159	9.885	957.42
FLAHS	0.199	10.910	1166.58
FUAHS	0.150	4.732	518.36

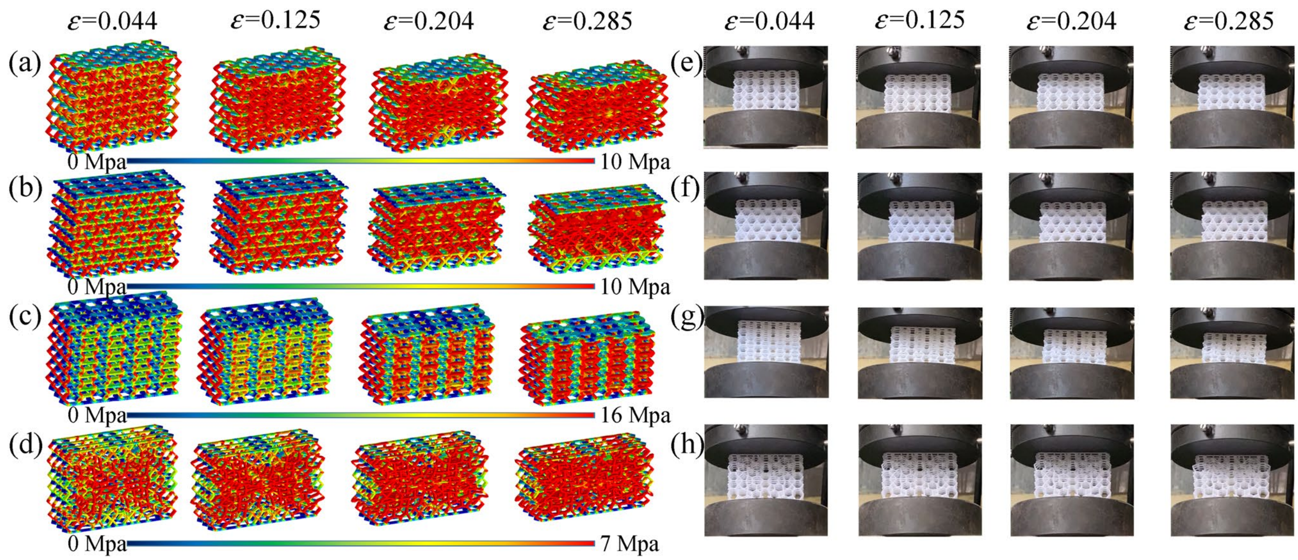

Fig. 7 The deformation and stress of honeycomb arrangement structures. **a–d** RAHS, SAHS, FLAHS, and FUAHS stress distribution diagrams at compression strain of 0.044, 0.105, 0.204, 0.245. **e** RAHS, SAHS, FLAHS, and FUAHS deformation diagrams of compression experiments

CPF is the maximum force during the deformation of bio-inspired structures and is calculated as Eq. (42):

$$\mathrm{CPF} = \max\left(F(x)\right), \tag{42}$$

CMF is the average force during the compression of the structure and is calculated using Eq. (43):

$$\mathrm{CMF} = \frac{1}{x_0}\int_0^{x_0} F(x)dx = \frac{EA}{x_0}. \tag{43}$$

Eventually, CFE refers to the homogenization of the force–displacement curve. CFE is the percentage of CMF to CPF [32], as presented by Eq. (44).

$$\mathrm{CFE} = \frac{\mathrm{CMF}}{\mathrm{CPF}} \times 100\,\% \tag{44}$$

This value is presented as a percentage and *CFE* of 100% is optimal and well-distributed energy absorption has taken place.

4.2 Properties Analysis of Bionic Honeycomb Arrangement Structures

To study the energy absorption and protection performance of four honeycomb arrangement structures, simulations and experiments are carried out. Before conducting simulations, the models are gridded with four-node elements. The freedom of the bottom surface is constrained, that is, the models are placed in a fixed position and are compressed. To obtain accurate deformation and response effect, contact conditions are set for the simulation model. #Auto-Surface Contact and #Single Surface Contact are used for simulations. The friction coefficient between structures is set as 0.2. The deformation comparison of honeycomb arrangement structures is as shown in Fig. 7a–d.

It can be seen from Fig. 7 that the models' deformation of simulations is consistent with the deformation in the experiments, which verifies the effectiveness of simulations. Due to the uniform compression of the rigid wall, the four honeycomb arrangement structures show progressive bending failure. FLAHS and FUAHS show overall uniform failure, while RAHS and SAHS show hierarchical failure. It can be clearly seen from Fig. 7 that RAHS and SAHS present hierarchical failure. The whole deformation of FLAHS is uniform when the structure is compressed, and FUAHS is 'X'-type failure. This phenomenon is caused by the defects such as geometrical gaps and holes in the sample preparation [33]. The hierarchical failure is observed. It can be found that the structural failure has regularity, and the dense part of the failure has an obvious regularity, that is, the large part of the void is prone to structural failure. In the later stage, the failure effect will be further studied, and the induced failure effect will be achieved by designing the structure through the hierarchical failure phenomenon. This special regularity can be applied to structural design, and the failure point of impact structure can be preset to meet the engineering needs.

The mechanical properties' curves of honeycomb arrangement structures in quasi-static compression experiments, simulations' analysis, and theoretical analysis are shown in Fig. 8.

It can be seen from Fig. 8a that the force–displacement curves of all structures are basically similar in shape. In general, the force–displacement curve of the structure can be divided into three different stages: (1) Elastic stage, (2) yield

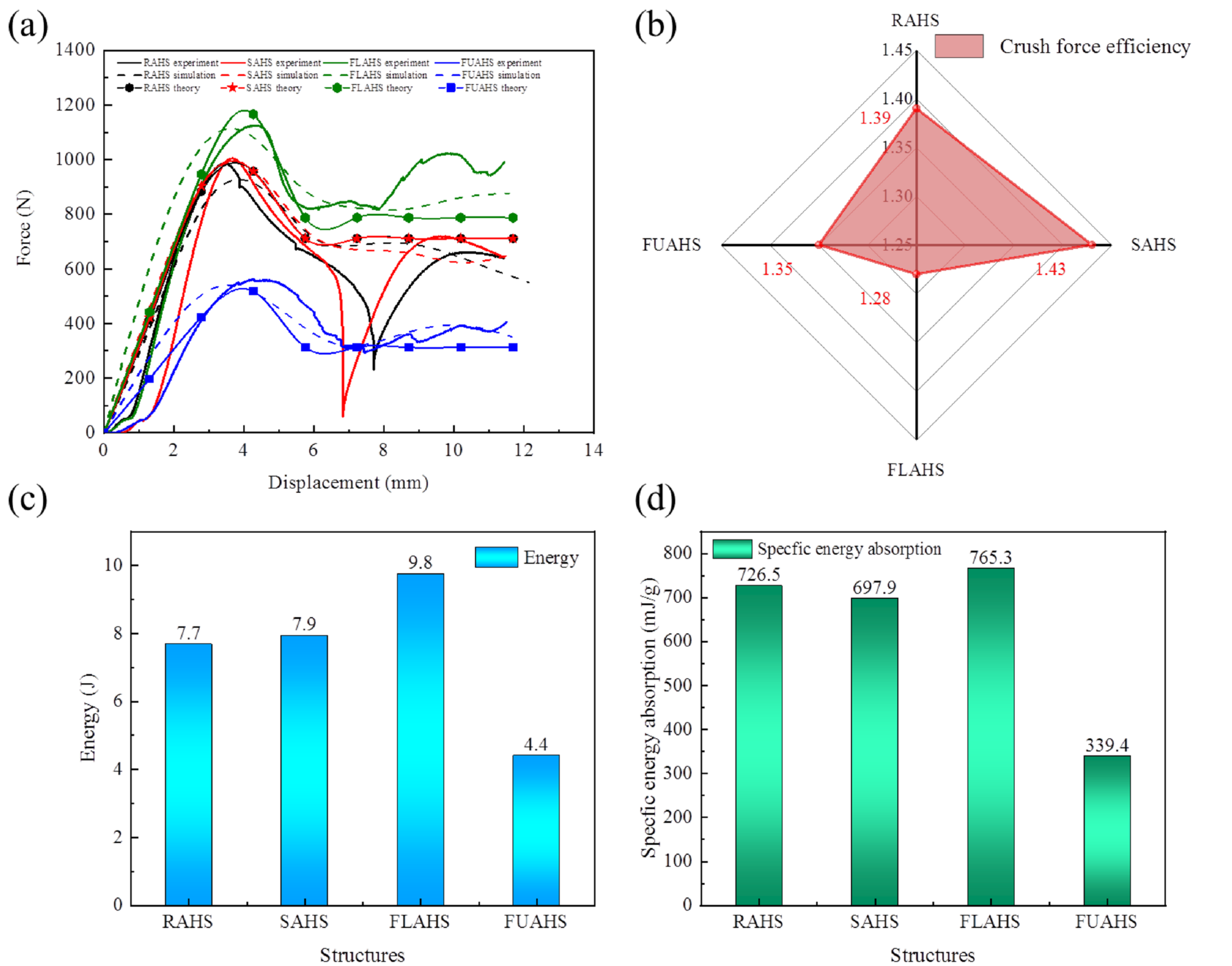

Fig. 8 The mechanical characteristic curves of honeycomb arrangement structures. **a** The experiment, simulation and theoretical Force–Displacement curves of honeycomb arrangement structures. **b** CFE radar figure of four honeycomb arrangement structures. **c** EA histogram of honeycomb arrangement structures. **d** SEA histogram of honeycomb arrangement structures

stage, (3) platform stage. From the perspective of crashworthiness, FLAHS have higher bearing capacity than those of RAHS, SAHS and FUAHS. The maximum force of RAHS, SAHS, FLAHS, and FUAHS is 956 N, 1031 N, 1138 N, and 596 N, respectively. The maximum force of FUAHS is 62.3%, 57.8%, 52.4% of RAHS, SAHS and FLAHS. Because of CFE_{FLAHS} and CFE_{FUAHS} is close to 1, FLAHS and FUAHS have higher structural stability. FLAHS has the strongest SEA, and its SEA is 105.3%, 109.6%, 225.4% of RAHS, SAHS, and FUAHS and its EA is 126.95%, 122.85%, 221.45% of RAHS, SAHS and FUAHS.

From the perspective of bionic functionalization, it can be seen from Fig. 8a that RAHS and SAHS inherit the advantages of high strength at the tip and middle part of the Gideon beetle, but at the same time, they also have the disadvantage of bending and brittle fracture. As can be seen from Fig. 7e, f, the fracture position of RAHS and SAHS shows class fracture failure, that is, RAHS and SAHS have the effect of induced interlayer failure. Induce damage by controlling structures. FLAHS and FUAHS perfectly inherit the stable force properties of compression in the shard and abdomen of the Gideon beetle, and the high strength in the shard is better. The excellent characteristics of biological structures can provide ideas for structural design objectives of engineering applications and greatly simplify the process of optimal design.

5 Conclusion

In this paper, RSM and PSO are used to optimize bio-inspired cells for finding the optimal honeycomb cell's size. Based on optimal cells, four kinds of bio-inspired honeycomb arrangement structures are designed based on the horn, the shard, and the abdominal layers of the

Gideon beetle. The crashworthiness and energy absorption properties of bio-inspired structures are experimented, simulated, and theoretically analyzed. According to Euler theory and buckling failure theory, compression properties of bio-inspired structures are fully explained. The theoretical analysis results have high accuracy and the error is guaranteed to be within 10%. In view of the results, the four honeycomb arrangement structures exhibit different bearing capacities. The maximum force of FUAHS is 62.3%, 57.8%, 52.4% of RAHS, SAHS and FLAHS. From the perspective of EA, the maximum EA of FLAHS is increased by 26.95%, 22.85%, and 121.45% than others, respectively. Four bio-inspired structures inherit the functional properties of different parts of the Gideon beetle. This method, designing bio-inspired structures with biological functions, can be introduced into the engineering field requiring the special function.

Supplementary Information The online version contains supplementary material available at https://doi.org/10.1007/s42235-022-00176-2.

Acknowledgements This research is funded by the National Key R&D Program of China (No. 2018YFB1105100), the National Natural Science Foundation of China (No. 51975246), Science and Technology Development Program of Jilin Province (YDZJ202101ZYTS134), the Ascl-zytsxm (202013), the Open Project Program of Key Laboratory for Cross-Scale Micro and Nano Manufacturing, Minstry of Education, Changchun University of Science and Technology (CMNM-KF202109), the Program for JLU Science and Technology Innovative Research Team (No. 2019TD-34), Jilin Scientific and Technological Development Program (20200404204YY), Interdisciplinary Research Fund for Doctoral Postgraduates of Jilin University (No.101832020DJX052), Interdisciplinary Cultivation Project for Young Teachers and Students (No. 415010300078).

Author Contributions RL conceptualization, supervision, writing review and editing. GY review. ZX review. XG: assisted with sampling analyses. KG assisted with sampling and laboratory analyses. QC investigate and survey. ZY supervision, writing review and editing. ZZ writing review and editing. CH proofread the format and language. JL recommends and provide relevant references. All authors read and approved the final manuscript.

Availability of Data and Materials The data and materials that support the findings of this study are available from the corresponding author upon reasonable request.

Declarations

Conflict of Interest We declare that we have no financial and personal relationships with other people or organizations that can inappropriately influence our work, there is no professional or other personal interest of any nature or kind in any product, service and/or company that could be construed as influencing the position presented in, or the review of the manuscript entitled.

Ethics Approval and Consent to Participate Not applicable.

Consent for Publication Not applicable.

References

1. Kumar, S., Parakkal, J., Rajkumar, A., Schiffer, A., & Deshpande, V. (2019). Tunable energy absorption characteristics of architected honeycombs enabled via additive manufacturing. *ACS Applied Materials & Interfaces, 11*, 42549–42560.
2. Ma, Y., Sugahara, T., Yang, Y., & Hamada, H. (2015). A study on the energy absorption properties of carbon/aramid fiber filament winding composite tube. *Composite Structures, 123*(5), 301–311.
3. Yang, X., Sun, Y., Yang, J., & Pan, Q. (2018). Out-of-plane crashworthiness analysis of bio-inspired aluminium honeycomb patterned with horseshoe mesostructure. *Thin-Walled Structures, 125*(4), 1–11.
4. Zhang, J., Karagiozova, D., Lu, G., & Chen, P. (2020). Quasi-static in-plane compression of zig-zag folded metamaterials at large plastic strains. *Thin-Walled Structures, 159*(2), 107285.
5. Du, J., & Peng, H. (2018). Investigation on microstructure of beetle elytra and energy absorption properties of bio-inspired honeycomb thin-walled structure under axial dynamic crushing. *Nanomaterials, 8*(9), 667.
6. Peng, H., & Du, J. (2018). Energy absorption characteristics of bio-inspired honeycomb column thin-walled structure under impact loading. *Journal of Behavior of Biomedical Materials, 79*, 301.
7. Li, K., Gao, X. L., & Wang, J. (2007). Dynamic crushing behavior of honeycomb structures with irregular cell shapes and non-uniform cell wall thickness. *International Journal of Solids and Structures, 44*(14–15), 5003–5026.
8. Tejavibulya, N., Youssef, J., Bao, B., Ferruccio, T. M., & Morgan, J. R. (2011). Directed self-assembly of large scaffold-free multi-cellular honeycomb structures. *Biofabrication, 3*(3), 034110.
9. Wei, Z., & Xu, X. (2021). Gradient design of bio-inspired nacre-like composites for improved impact resistance. *Composites Part B Engineering, 215*(5), 108830.
10. Xiang, X., Zou, S., Ha, N. S., Lu, G., & Kong, I. (2020). Energy absorption of bio-inspired multi-layered graded foam-filled structures under axial crushing. *Composites Part B Engineering, 198*, 108216.
11. Liu, Q., Ma, J., He, Z., Hu, Z., & Hui, D. (2017). Energy absorption of bio-inspired multi-cell CFRP and aluminium square tubes. *Composites Part B Engineering, 121b*(7), 134–144.
12. Zhang, W., Yin, S., Yu, T. X., & Xu, J. (2019). Crushing resistance and energy absorption of pomelo peel inspired hierarchical honeycomb. *International Journal of Impact Engineering, 125*(4), 163–172.
13. Tang, C. Y., Tsui, C. P., Wei, L., & Wang, Z. W. (2011). Damage analysis on a graded porous biocomposite structure under flexural load using FEM. *Strength, Fracture and Complexity, 7*(3), 241–252.
14. Liu, D. X., Qing-He, H. E., Yuan, W. H., & Liu, J. H. (2011). Analysis of quasi-static compression energy absorption of thin-wall cylindrical energy absorption device. *Electric Locomotives & Mass Transit Vehicles, 24*(3), 341–354.
15. Mencattelli, L., & Pinho, S. T. (2020). Ultra-thin-ply CFRP bouligand bio-inspired structures with enhanced load-bearing capacity, delayed catastrophic failure and high energy dissipation capability. *Composites Part A: Applied Science and Manufacturing, 129*, 105655.
16. Ashby, M. F., & Gibson, L. J. (1997). *Cellular solids: structure* (pp. 175–231). Properties and Applications. Press Syndicate of the University of Cambridge.
17. Wei, K., Peng, Y., Qu, Z., Zhou, H., Pei, Y., & Fang, D. (2018). Lightweight composite lattice cylindrical shells with novel character of tailorable thermal expansion. *International Journal of Mechanical Sciences, 137*, 77–85.

18. Gibson, L. J., & Ashby, M. F. (1982). The mechanics of three-dimensional cellular materials. *Proceedings of the Royal Society of London Series A Mathematical and Physical Sciences, 382*(1782), 43–59.
19. Zhang, X. C., Liu, Y., & Zhang, Z. M. (2009). Research on dynamic properties of supercell honeycomb structures under impact loading. *Chinese Engineering Mechanics, 26*(06), 220–225.
20. Chen, D. H., & Masuda, K. (2017). Estimation of stress concentration due to defects in a honeycomb core. *Engineering Fracture Mechanics, 172*, 61–72.
21. Asprone, D., Auricchio, F., Menna, C., Morganti, S., Prota, A., & Reali, A. (2013). Statistical finite element analysis of the buckling behavior of honeycomb structures. *Composite Structures, 105*, 240–255.
22. Wang, S. L., Wang, H. Q., Ding, Y. Y., & Yu, F. (2020). Crushing behavior and deformation mechanism of randomly honeycomb cylindrical shell structure. *Thin-walled structures, 151*, 106739.
23. Stefan, J., & Markus, B. (2017). Application of 3D (color) printing for the visualization and optimization of complex metal forming processes. *Procedia Engineering, 207*, 1081–1086.
24. Günther, D., Heymel, B., Günther, J. F., & Ederer, I. (2014). Continuous 3D-printing for additive manufacturing. *Rapid Prototyping Journal, 20*(4), 320–327.
25. Kruth, J. P., Leu, M. C., & Nakagawa, T. (1998). Progress in additive manufacturing and rapid prototyping. *CIRP Annals-Manufacturing Technology, 47*(2), 525–540.
26. Lu, L. Z., Tian, Y. B., Cai, Y. C., Xin, Y., Chen, X. Y., Zhang, G. Y., & Han, J. (2021). Microstructure and mechanical properties of a functionally graded material from TA1 to Inconel 625 fabricated by dual wire + arc additive manufacturing. *Materials Letters, 298*, 130010.
27. Liu, X., Zhou, Z., Guirao, J. L. G., & Wei, G. (2017). A novel prediction model based on particle swarm optimization and adaptive neuro-fuzzy inference system. *Journal of Intelligent & Fuzzy Systems, 33*(5), 3137–3143.
28. Yu, H. L., Gao, Y. L., Wang, L., & Meng, J. T. (2020). A hybrid particle swarm optimization algorithm enhanced with nonlinear inertial weight and Gaussian mutation for job shop scheduling problems. *Mathematics-Basel, 8*(8), 1355.
29. Manoj, I. V., Narendranath, S., & Pramanik, A. (2021). Optimization and prediction of machining responses using response surface methodology and adaptive neural network by wire electric discharge machining of alloy-x. *Materials Science Forum, 1026*, 28–38.
30. Chen, J. X., Ni, Q. Q., Xu, Y. L., & Iwamoto, M. (2006). Lightweight composite structures in the forewings of beetles. *Composite Structures, 79*(3), 331–337.
31. Chen, J. X., Dai, G. Z., Xu, Y. L., & Iwamoto, M. (2006). Optimal composite structures in the forewings of beetles. *Composite Structures, 81*(3), 432–437.
32. Simpson, J., & Kazanc, Z. (2020). Crushing investigation of crash boxes filled with honeycomb and re-entrant (auxetic) lattices. *Thin-Walled Structures, 150*, 106676.
33. Chen, S., Tan, X., Hu, J., Zhu, S., & Wu, L. (2021). A novel gradient negative stiffness honeycomb for recoverable energy absorption. *Composites Part B Engineering, 215*, 108745.
34. Wang, T., An, J., He, H., Wen, X., & Xi, X. (2021). A novel 3D impact energy absorption structure with negative poisson's ratio and its application in aircraft crashworthiness. *Composite Structures, 262*, 113663.